Comparison of Observed Divertor Heat Flux and Modeling Results at LHD*)

Peter DREWELOW, Suguru MASUZAKI[1)], Sergey BOZHENKOV, Yuehe FENG, Marcin W. JAKUBOWSKI, Yasuhiro SUZUKI[1)], Robert WOLF, Hiroshi YAMADA[1)] and LHD Experiment Group

Max-Planck-Institut für Plasmaphysik, EURATOM Assoziation, 17491 Greifswald, Germany
[1)]*National Institute for Fusion Science, Toki 509-5292, Japan*

(Received 22 November 2012 / Accepted 26 June 2013)

The divertor strike line pattern on the helical divertor of LHD was observed with an infra red camera. The derived heat flux pattern show multiple distinct strike lines depending on the equilibrium magnetic configuration. Predictions of such divertor heat loads thus require a modeling of the magnetic configuration and the heat transport in the magnetic edge. Equilibrium magnetic topologies were analyzed with HINT2, while the plasma fluid model code EMC3 was used to simulate the energy transport in the edge. The measured multi peak structure of the divertor heat flux is correlated to the intersection points of elongated loop shaped flux tubes of long L_C field lines. But the fluid model could not recreate the total energy load and the multiple heat flux peaks on the divertor. A Variation in the plasma density n_e as a transport parameter in order to fit the simulated heat flux to the measured one shows a contradicting tendency.

Keywords: LHD, helical divertor, strike line pattern, finite beta, stochastic field lines, HINT2, EMC3

DOI: 10.1585/pfr.8.2402126

1. Introduction

The divertor as the designated plasma wall contact area has to withstand enormous heat loads of the order of 1 MW/m^2 in modern fusion experiments, like the Large Helical Device (LHD) [1]. Future experiments like Wendelstein 7-X and ITER are expected to expose these wall components to stationary heat loads of up to 10 MW/m^2 or 15 MW/m^2, respectively [2, 3]. This will meet or exceed today's technical limits for common divertor materials and pose a challenge to the material science. In the process of planning these next step fusion experiments, it becomes essential to predict the divertor heat loads in their absolute value and the distribution on the divertor surface.

In the case of LHD, the strike line structure on the helical divertor [4] is influenced by the complex magnetic edge topology. Previous attempts [5] to verify numerical models of the divertor heat flux at LHD with Langmuir probe measurements showed good qualitative agreement. Changes in different density regimes could be correlated to changing cross field transport. In this work, the modeling of divertor heat loads on the helical divertor of LHD is cross checked with experimental observations using a high resolution infra red camera in order to investigate the influence of magnetic edge stochastization.

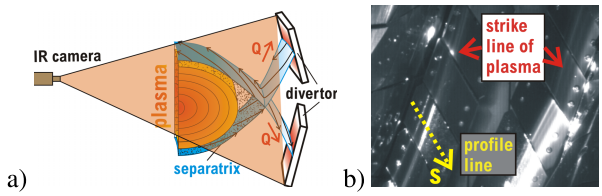

Fig. 1 a) Setup of the infra red camera observing the inboard side divertor at LHD. b) Infra red image with line s as region of interest.

2. Measurement at LHD

The helical divertor of LHD was observed with an infra red camera sensitive in a spectral range of $\lambda = 3$ - 5 µm, a spatial resolution of $\Delta x = 3.5$ mm and a temporal resolution of $\Delta t = 10$ ms. Observed was the central inboard side divertor section from the outboard side, as shown in Fig. 1 a). For this line integrating view infrared radiation from the plasma is neglected in this wavelength range. A profile line s perpendicular to the strike line and on the surface of one divertor tile was defined as the region of interest (see Fig. 1 b)). The heat flux density has been derived at this location. A two-dimensional (2D) thermal transport model code called THEODOR [6] was applied to derive the incoming heat flux $Q_{\mathrm{plasma}}(s,t)$ from the divertor surface temperature $T(s,t)$ by solving the heat propagation equations in the divertor tile. Thin surface layers with partial thermal insulation from the bulk of the divertor tile

author's e-mail: peter.drewelow@ipp.mpg.de
*) This article is based on the presentation at the 22nd International Toki Conference (ITC22).

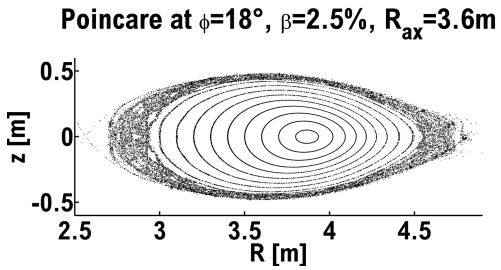

Fig. 2 Poincare plot of a magnetic equilibrium at $\beta = 2.5\%$ at LHD.

were taken into account by iteratively optimizing a surface heat transfer coefficient.

3. Modeling Tools

3.1 HINT2

The magnetic topology in a heliotron like LHD is in the first order defined by the external magnet coils. Nevertheless, plasma currents in a finite β plasma influence the vacuum magnetic field. A reliable prediction of the magnetic topology can be provided by HINT2 [7], a three-dimensional (3D) magneto hydro-dynamic equilibrium code. Unlike other common equilibrium codes (e.g. VMEC), HINT2 does not assume nested flux surfaces or has fixed boundary constraints. It can therefore include edge ergodization, which is supposed to be important for the magnetic topology at the divertor. The HINT2 algorithm starts with a given vacuum magnetic field and plasma pressure distribution on a 3D grid and proceeds with an iteration of two steps. First, a relaxation of the plasma pressure in a fixed magnetic field and second, a relaxation of the magnetic field with fixed pressure. When the changes after an iteration step are small enough, a convergence to equilibrium is assumed.

The magnetic field was analyzed using a numeric field line tracer in order to follow field lines from a start point to intersection points e.g. in a φ = const. plane (Poincare plot) or on a triangular mesh model of the plasma vessel or divertor. Figure 2 shows as an example Poincare plot of the LHD magnetic field in a high β equilibrium calculated with HINT2. It shows all the prominent features expected for an equilibrium with high plasma β. The volume of stochastic edge field lines is large, various island structures appear in the edge outside the intact flux surfaces and the center magnetic flux surfaces exhibit a Shafranov shift in major radius direction.

3.2 EMC3

In order to interpret the measured heat flux distribution on the divertor the fluid model of EMC3 [8] has been applied. The computational mesh of EMC3 is constructed along the field lines of the magnetic equilibrium from HINT2. Due to the stochastic nature of the edge magnetic field, this mesh becomes increasingly non-uniform going to the very edge and the divertor legs. Numerical singularities prevent an extension of this grid until the helical divertor of LHD. Therefore, the self consistent modeled power flux in the stochastic zone is only calculated in a limited edge region as shown in Fig. 3 a).

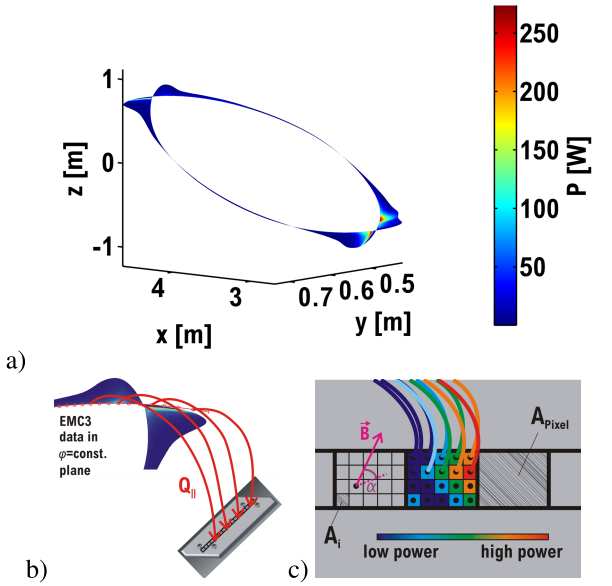

Fig. 3 a) Power flux in the edge calculated by EMC3. b) Principle of projecting $Q_{\parallel}$ from the computational mesh of EMC3 to the divertor. c) Inhomogeneous power deposition on each pixel of the divertor profile line s.

The parallel heat flux $Q_{\parallel}$ is assumed to follow the magnetic field lines going from the EMC3 computational mesh to the divertor (distance $\approx$ 3 m) without further diffusion (see Fig. 3 b)). Since the modeled heat flux is to be compared to the measured flux along a divertor profile line s (see Fig. 1 b)), only a resolution along this line according to the pixel size of the infra red camera is of interest. However, as shown in Fig. 3 c), the distribution of power loads onto a pixel can be inhomogeneous. Connecting the center point of each pixel by field line tracing with the EMC3 computational mesh is not enough. Field lines from 900 sub-pixel areas A_i where traced to the EMC3 data plane. Each field line provides a power contribution $P_i = Q_{\parallel,i} \cdot A_i \cdot \sin\alpha_i$, with α being the angle between the B field vector and the divertor surface. The modeled heat flux $Q_{\mathrm{EMC3}}(s)$ at one pixel is then the sum of all power contributions divided by each pixel area A_{Pixel}.

4. $Q(s)$ and the Magnetic Topology

As a first order comparison to the measured heat flux profile $Q(s)$ the connection length L_C of field lines starting along the profile line s was calculated. Figure 4 shows such a comparison for a plasma experiment with plasma $\beta = 1\%$. Experimental conditions were: magnetic field strength of $B_{\mathrm{ax}} = 2$ T, magnetic axis position at

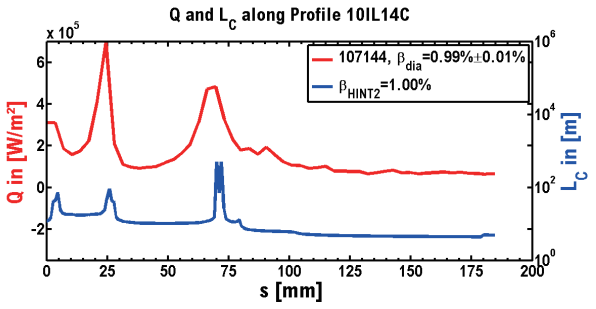

Fig. 4 Measured heat flux and calculated connection length of field lines along s for $\beta = 1\%$.

$R_{ax} = 3.6\,\mathrm{m}$, central density of $n_e \approx 2.9 \cdot 10^{19}\,\mathrm{m}^{-3}$ and NBI heating of $P_{input} \approx 8\,\mathrm{MW}$. The strong correlation between the heat load peak structure in $Q(s)$ and the pattern of long field lines indicates that the long L_C field lines carry the main power flux from the last closed flux surface (LCFS) to the divertor, as seen also on Tokamaks (e.g. DIII-D or TEXTOR). On LHD it is caused by the fact, that the long L_C field lines repeatedly approach the LCFS, while short field lines get close to the LCFS only once or twice.

The occurrence of the observed multiple heat flux peaks as well as the localization on long L_C field lines depend on the plasma β. Thus, the stochastic edge topology which changes with higher β seems to directly affect the strike line pattern on the divertor, although the divertor is far off from the plasma. This contradicts the common assumption that only the near field of the helical field coils determines the divertor strike line pattern.

In order to understand the local L_C pattern presented in Fig. 4 it is necessary to analyze the L_C distribution over the complete inboard divertor. Figure 5 a) shows the pattern of long L_C field lines derived by field line tracing from the whole inboard half of the helical divertor going from the top of the LHD ($\theta = 90°$), passing the horizontal plane ($\theta = 180°$) until the bottom of LHD ($\theta = 270°$). Helically inhomogeneous flux tube structures (so called 'whiskers') stretch over both helical divertors. In Fig. 5 b) it becomes obvious, that the location of the measured maxima in the $Q(s)$ profile is correlated to these whiskers in the mid-plane region.

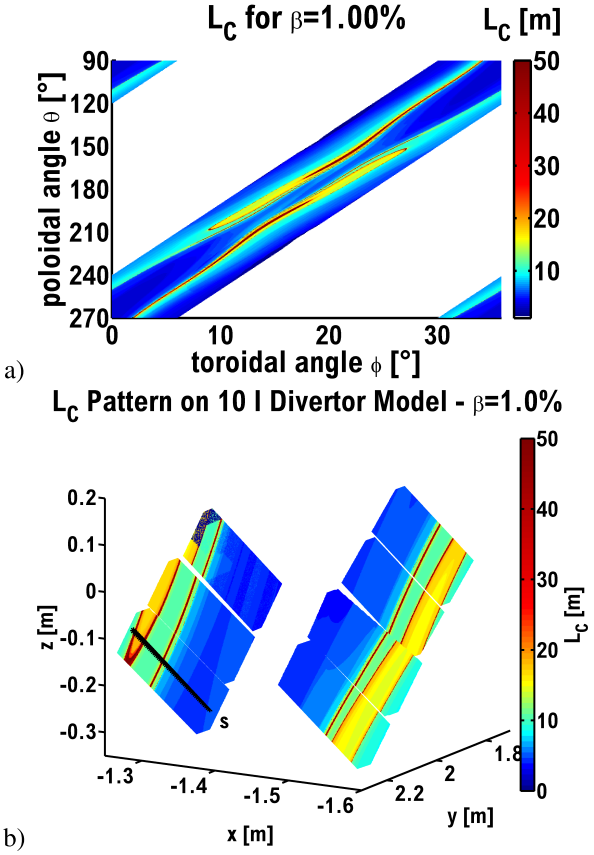

Fig. 5 Connection length of field lines along the helical divertor. Plot a) ranges from the top, over the inboard side to the bottom of the machine and b) shows the pattern on the observed divertor tiles.

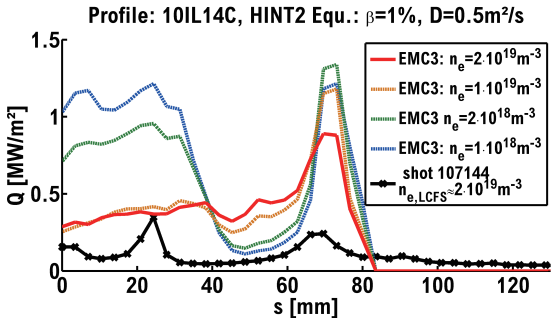

Fig. 6 Heat flux along divertor line s modeled by EMC3 for various values of the edge density parameter n_e.

5. Simulated Heat Flux

Apart from the analysis of the magnetic topology at the divertor, the application of EMC3 also allows to check for transport driven effects on the $Q(s)$ profile. From first principle assumptions, the transport should affect peak heights and widths rather than the peak locations. A simulation of the heat flux along the divertor profile s with similar condition as in the experiment ($P_{input} \approx 8\,\mathrm{MW}$, $n_e \approx 2 \cdot 10^{19}\,\mathrm{m}^{-3}$ in the edge) is shown in Fig. 6 as the red graph. The location of the main peak at ca. $s = 72\,\mathrm{mm}$ fits to the experimental data (see black solid line in Fig. 6). But the total level of heat flux is much higher in the simulation and the measured maxima in Q on the left hand side could not be modeled with EMC3.

One explanation for the missing heat flux peaks could be a too strong perpendicular energy transport. Since the density n_e affects the energy diffusion in the ECM3 model, a scan of this parameter was conducted. Reducing the electron density (from red graph to blue graph in Fig. 6) has two effects:

1. The total heat flux increases as the perpendicular en-

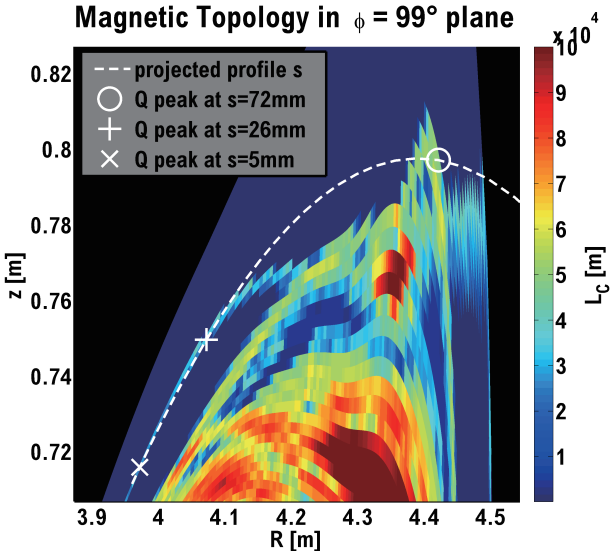

Fig. 7 Divertor profile line s projected along field lines to φ = 99°-plane and the projection of the three main $Q(s)$ peaks in Fig. 4.

ergy diffusion is reduced in favor of the parallel transport.

2. The Q peaks on the left hand side appear since a reduced energy diffusion can no longer smear out the heat flux peaks at the long L_C field lines.

Regarding the second effect, the left hand side heat flux peaks turned out to be more sensitive to the assumed energy diffusion during the modeling with the EMC3 code. In order to understand this, it is important to compare the magnetic topology surrounding the field lines related to the three Q peaks. Field lines starting from the divertor profile line s were traced to the φ = 99°-plane of the EMC3 computational mesh. Figure 7 shows a part of the φ = 99° plane with white marks on the intersection points of field lines starting from the three Q peaks of Fig. 4. The dashed line in Fig. 7 can be understood as the projected divertor profile line s into the φ = 99°-plane. The magnetic topology in this plane is visualized by the connection length pattern. The long L_C field line at the $s \approx 72$ mm peak ('o' marker in Fig. 7) belongs to a broad flux tube of long L_C field lines. Energy diffusion will distribute quantities of the parallel heat flux to the neighboring long field lines, which all ultimately end in the vicinity of the $s \approx 72$ mm peak. On the other hand, the field lines from the other Q peaks are located on a very thin elongated flux tube adjacent to short L_C field lines. These short L_C field lines act as energy sinks guiding the diffused energy directly to other parts of the divertor or plasma vessel.

6. Conclusions

The divertor heat flux pattern at LHD has a strong correlation to the magnetic topology characterized by the connection length of field lines. Elongated flux tubes with long L_C field lines show whisker shaped intersection pattern on the divertor, which are responsible for multiple local heat flux maxima on the divertor tile. The MHD fluid code EMC3 used to simulate the divertor heat flux pattern has difficulties modeling these multi-peak structures as observed in the experiments. Parameter scans in this modeling indicate that some of the heat flux maxima require low energy diffusion, while an overall divertor heat flux similar to the observed one requires high energy diffusion.

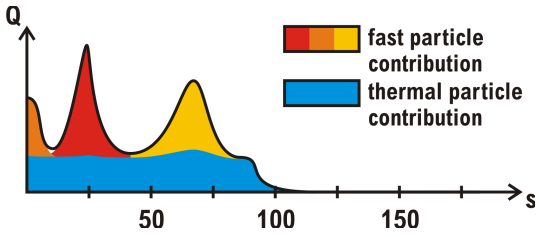

Fig. 8 Interpretation of sources of energy in the multi peak Q profile.

A possible interpretation of this result is the existence of two groups of plasma particles with different perpendicular transport. One group carries most of the energy to the divertor and exhibits strong energy diffusion. Due to a strong broadening, the resulting heat flux is deposited on the divertor nearly in form of a step function as sketched in Fig. 8. A second group of particles (probably fast electrons) with a mean free path longer than the length of field lines connecting the LCFS with the divertor shows nearly no energy diffusion. They would transport energy directly to the intersection points of those long field lines with the divertor, forming distinct peaks. A similar effect has been found for Langmuir probes on the divertor of DIII-D [9]. A mean free path correction for T_e was deemed necessary because of the fast electron contribution to the probe current.

The fluid model of EMC3 assumes a thermal equilibrium, i.e. the fast electrons in the high energy tail of the Maxwell distribution have enough interactions in order to share their energy with other electrons. If, however, fast electrons have a measurable impact, a gyro-kinetic transport model is necessary to correctly simulate the divertor heat flux pattern.

[1] O. Motojima *et al.*, Nucl. Fusion **43**, 1674 (2003).
[2] H. Renner *et al.*, Fusion Sci. Technol. **46**, No.2, 318 (2004).
[3] A. Herrmann *et al.*, J. Nucl. Mater. **313-316**, 759 (2003).
[4] N. Ohyabu *et al.*, Nucl. Fusion **34**, No.3, 387 (1994).
[5] S. Masuzaki *et al.*, Contrib. Plasma Phys. **50**, No.6-7, 629 (2010).
[6] A. Herrmann *et al.*, ECA **25A**, 2109 (2001).
[7] Y. Suzuki *et al.*, Nucl. Fusion **46**, L19 (2006).
[8] Y. Feng *et al.*, J. Nucl. Mater. **266-269**, 812 (1999).
[9] J.G. Watkins *et al.*, J. Nucl. Mater. **290-293**, 778 (2001).